THE JOURNAL OF PHYSICAL CHEMISTRY C

ARTICLE

pubs.acs.org/JPCC

Pristine and Hybrid Nickel Nanowires: Template-, Magnetic Field-, and Surfactant-Free Wet Chemical Synthesis and Raman Studies

K. R. Krishnadas, P. R. Sajanlal, and T. Pradeep*

DST Unit of Nanoscience, Department of Chemistry and Sophisticated Analytical Instrument Facility, Indian Institute of Technology, Madras, Chennai 600 036, India

Supporting Information

ABSTRACT: Nickel nanowires of high purity and various aspect ratios were synthesized by a wet chemical reduction method without the assistance of surfactants, templates, and external magnetic field. The observed unique optical absorption features of nickel nanowires are highly dependent on the nanowire dimensions. In order to tailor the physical and chemical properties of the nanowires, we have incorporated functionalities in the form of tellurium and zinc oxide coating on them by overgrowth processes using simple wet chemical reactions. The pristine and functional nanowires were characterized by different microscopic and spectroscopic techniques such as scanning electron microscopy (SEM), transmission electron microscopy (TEM), confocal Raman microscopy, X-ray diffraction spectroscopy (XRD), and UV−visible spectroscopy. Our system provides additional details into the growth of anisotropic Ni nanowires, especially in the absence of surfactants, templates, and external magnetic field. We have also demonstrated surface-enhanced Raman scattering (SERS) activity of the Ni nanowires using crystal violet as the probe molecule.

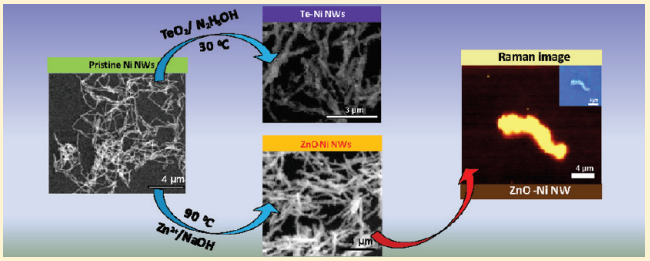

1. INTRODUCTION

Anisotropic nanostructures of metals are extensively studied due to their size- and shape- dependent properties and interesting growth mechanisms. Usually materials based on noble metals are investigated in this context, although anisotropic nanostructures of other transition metals are also prepared. Spherical as well as anisotropic magnetic nanoparticles are of great interest due to potential applications like magnetic data storage,[1] magnetic fluids,[2] and biomedical purposes,[3] etc. Nickel nanowires (NWs), rods,[4,5] tubes,[6,7] flowers,[8] and triangles[9] were synthesized by different groups. Among these anisotropic structures, NWs are studied extensively, presumably due to the ease of synthesis. Catalytic activity of Ni NWs is utilized for the conversion of methane to synthesis gas.[10] Even though Ni NWs have been used for various applications in biology, including cell and protein separation,[11−13] the biocompatibility and cytotoxicity of Ni nanoparticles is still under investigation. Magnetic properties of the Ni NWs have been extensively investigated by many groups.[14−17]They are expected to be useful in high-density magnetic data storage.

Advances in synthetic methods provide numerous possibilities for obtaining novel functional materials with highly controlled morphology and composition, useful for practical applications. Two-component triblock magnetic nanorods composed of Au and Ni were synthesized by templated methods and used for efficient separation of protein mixtures.[18,19] Spherical nanoparticles and NWs of alloys like Ni/Fe,[20] Co/Ni[21,22] and Ni/γ-Fe_2O_3[23] were prepared by template-assisted methods. Bimetallic core−shell nanorods like Ni@Co[24] were prepared by template-assisted methods. Uniform Cu@Ni nanorods of well-defined composition were synthesized by a surfactant-assisted one-pot wet-chemical method.[25] Hybrid metal−semiconductor nanomaterials are expected to show novel electronic properties. Te and ZnO nanostructures are widely studied systems due to their interesting physical and chemical properties.[26] Tellurium is a p-type semiconductor that exhibits good nonlinear optical response, photoconductivity, piezoelectricity, and thermoelectric properties.[26a] ZnO is a direct wide band gap semiconductor and its nanocrystals find applications in optoelectronic devices and solar cells.[26b]

Ni NWs have been synthesized mainly by well-known template-assisted electrodeposition onto porous membranes.[27] Wet chemical syntheses of Ni NWs in solvents like water,[28] aqueous ethanol,[29,30] ethylene glycol,[31−35] and benzyl alcohol[36] have been reported. A serious limitation of these wet-chemical methods is the need to control several parameters like concentration of reagents, pH, surfactants, or external magnetic field to get NWs in good yield. Furthermore, use of surfactants and other chemicals decreases the purity of the material, which is necessary for several practical applications. Here, we demonstrate the synthesis of Ni NWs in high yield by a simple wet-chemical method without the assistance of any templates, surfactants, and

Received: November 3, 2010
Revised: January 23, 2011
Published: February 25, 2011

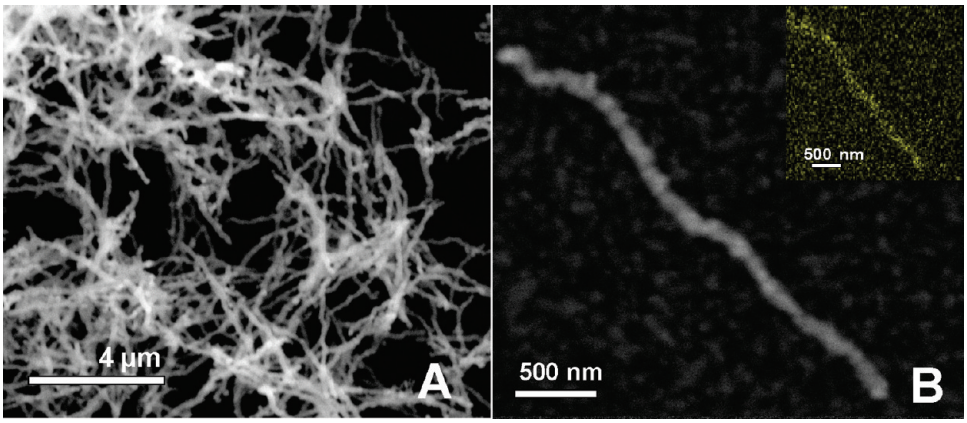

Figure 1. (A) Large-area SEM image of Ni NWs and (B) corresponding image of a single nanowire. (Inset) EDAX image due to Ni Lα of the single Ni NW shown in the SEM image.

external magnetic field. This provides an interesting system for the study of their growth mechanism where no surfactants or capping agents are needed for directed growth. In addition to these, we synthesized two types of functional NWs by overgrowing tellurium (Te) and zinc oxide (ZnO) on Ni NWs surfaces by wet-chemistry. ZnO coating on the Ni NWs will reduce their toxicity, which in turn may make them better suited for biological applications. We expect that these two hybrid NWs will exhibit novel magneto-optical characteristics due to the effective coupling of their magnetic and optical properties. Such magnetic material−semiconductor hybrid nanostructures are expected to be useful for spintronics. Also, these are interesting systems to study the growth of nanocrystals on preformed nanostructures, about which very little is known. We observed the surface-enhanced Raman spectroscopic (SERS) activity of the pristine Ni NWs using crystal violet as the probe molecule. Optical absorption of Ni NWs synthesized under various experimental conditions was also studied, and it was found that these features are highly dependent on the nanowire dimensions. Since the magnetic properties of the Ni NWs were extensively investigated by many groups, we did not focus on that aspect.

2. EXPERIMENTAL SECTION

2.1. Materials. Nickel chloride, ethylene glycol, zinc acetate dihydrate, and sodium hydroxide were purchased from SD Fine Chemicals, India (AR grade). Hydrazine monohydrate was purchased from Fisher Scientific (99−100%), and tellurium dioxide was purchased from Alfa Aesar (99.9%). All chemicals were used without further purification.

2.2. Synthesis of Nickel Nanowires. Ni NWs were synthesized by the reduction of nickel chloride in ethylene glycol as solvent with concentrated (99−100%) hydrazine hydrate solution as the reducing agent. In a typical procedure, 1 M aqueous solution of nickel chloride was prepared and the required volume of this solution was added to 7.5 mL of ethylene glycol in a glass bottle of 20 mL capacity to get a 10 mM solution of Ni^{2+}. The mixture was heated on a hot plate to 120 °C. About 0.5 mL of hydrazine hydrate solution was added rapidly into the hot solution at a stretch via a micropipet. No stirring was done during the whole process. Immediately after the addition of hydrazine, the whole solution turned black, forming a network kind of appearance throughout the bottle, and within 1 min, black Ni NWs were found floating over the liquid surface, leaving a clear solution below. NWs were separated by a magnet and washed thoroughly, first with distilled water and then with ethanol to remove excess hydrazine and solvent.

We synthesized Ni NWs at different Ni^{2+} concentrations such as 1.25, 2.50, 5.00, 10.00, and 25.00 mM. Required volumes of the standard nickel chloride solution (1 M) were added to 7.5 mL of ethylene glycol, via a micropipet, to prepare Ni^{2+} solutions of the above-mentioned concentrations. Slight changes in volume upon the addition of 1 M Ni^{2+} were disregarded in the calculation of final concentrations. To each of these solutions was added 0.5 mL of hydrazine hydrate, and the syntheses were carried out at 120 °C. A micropipet of 0.002 μL accuracy (Eppendorf) was used for the addition of very small volumes. We also prepared NWs with different amounts of hydrazine hydrate (100, 200, 300, and 500 μL) while keeping a Ni^{2+} concentration of 10 mM (in 7.5 mL ethylene glycol) at 120 °C. To understand the influence of temperature, NWs were prepared at 90, 120, and 160 °C (with 7.5 mL of 10 mM Ni^{2+} in ethylene glycol and 0.5 mL of hydrazine hydrate).

2.3. Synthesis of Tellurium-Coated Nickel Nanowires. The overgrowth of tellurium on Ni NW surface was done by reducing tellurium dioxide with hydrazine hydrate[37,38] in the presence of Ni NWs dispersed in ethylene glycol. In a typical procedure, 7.8 mg of TeO_2 and 1 mL of Ni NWs suspension in ethylene glycol (from the suspension of 2.8 mg of Ni NWs in 10 mL of ethylene glycol) were mixed in a 100 mL beaker, and 40 mL of water was added to it. Hydrazine hydrate solution (10 mL) was added at a stretch, and the mixture was sonicated for about 10 min. Reduction of TeO_2 was indicated by the appearance of light blue color to the solution. The clear solution was kept undisturbed for 1 h. Within 30 min after the addition of hydrazine, NWs started to settle from the solution. The NWs were separated from the free Te NWs formed in the bulk solution by a magnet and were washed with water and ethanol to remove excess reducing agents and other impurities.

2.4. Synthesis of Zinc Oxide-Coated Nickel Nanowires. In a typical procedure, 1 mL of Ni NW suspension in ethylene glycol (same as that used for Te coating) was added to 5 mL of 50 mM aqueous solution of zinc acetate, and the mixture was sonicated for 2 min. The mixture was heated to about 90 °C on a hot plate. To the hot solution, 5 mL of 0.2 M NaOH solution was added dropwise within about 10 min, and this mixture was kept at 90 °C for 1 h with occasional shaking. The product was separated by a magnet and washed with water and ethanol thoroughly, to

remove excess hydrazine and free ZnO particles formed in the solution.

3. INSTRUMENTATION

Scanning electron microscopy (SEM) imaging and energy-dispersive analysis of X-ray (EDAX) studies were done with a FEI QUANTA-200 scanning electron microscope. For SEM measurements, samples were drop-cast on an indium tin oxide-(ITO-) coated conducting glass and dried. Transmission electron microscopy (TEM) was carried out on a JEOL 3011, 300 kV instrument with an ultra-high-resolution (UHR) pole piece. Samples for TEM were prepared by dropping the dispersion on amorphous carbon films supported on a copper grid and drying the grids in air. UV−visible spectra of all of the samples were measured on a Perkin-Elmer Lambda 25 spectrometer by dispersing them in ethylene glycol. Raman measurements were done with a WiTec GmbH, Alpha-SNOM CRM 200 instrument having a 532 nm laser as the excitation source. The material was carefully transferred onto a cover glass, dried in air, and mounted on the sample stage of the Raman spectrometer. The back-scattered light was collected by a 100× objective at an integration time of 50 ms. A supernotch filter placed in the path of the signal effectively cuts off the excitation radiation. The signal was then dispersed by a 600 grooves/mm grating, and the dispersed light was collected by a Peltier cooled charge-coupled device (CCD). X-ray diffraction studies of the samples were done on a Bruker AXS, D8 Discover diffractometer using Cu Kα radiation at λ = 1.5418 Å.

4. RESULTS AND DISCUSSION

Figure 1shows (A) large-area and (B) single Ni nanowire images. The inset of Figure 1B shows the EDAX image of the single Ni NW due to Ni Lα. EDAX spectrum of the pristine Ni NWs is given in the Supporting Information (Figure S1). Dimensions and surface morphology of the wires could be controlled by adjusting the parameters such as concentration of the precursor, reducing agent, and temperature. It is interesting to note that NWs were formed exclusively and no spherical nanoparticles or other morphologies were obtained.

The NWs formed have good crystallinity, as revealed by XRD analysis (see later). EDAX and XRD analyses show that the presence of oxide layer on the nanowire surface was negligible. NWs with smaller dimensions could be dispersed for longer time in solvents like water and ethylene glycol, and dispersibility of the NWs decreased with increasing dimensions. To give an example, the NWs prepared with 1.25 mM Ni^{2+} (at 120 °C in ethylene glycol) were dispersed in ethylene glycol for about 2 h without settling, but the same sample of NWs started settling out of the aqueous dispersions after about 45 min. This is presumably due to the higher viscosity of ethylene glycol compared to water.

We prepared Ni NWs by conducting the experiment with 1.25, 2.50, 5.00, 10.00, and 25.00 mM Ni^{2+} solutions. Experimental conditions and results are summarized in Table 1 of the Supporting Information. The dimensions were reported from the analysis of about 50 individual NWs. An increase in the Ni^{2+} concentration resulted in an increase of both the diameter and the length of the NWs. Increase in length was much more apparent than increase in diameter. Average diameter of NWs synthesized at Ni^{2+} concentrations of 1.25, 5.00, and 10.00 mM were 60 ± 4, 100 ± 5, and 130 ± 7 nm, respectively. Even though a highly precise measurement of the length was not possible due to the nonlinearity of NWs, systematic changes were observed in the lengths of NWs prepared under different conditions. Also, lengths of a particular sample of NWs span a much wider range than the diameter. Lengths of these NWs were in the ranges of 1.50−2.00, 3.00−3.50, and 5.00−6.00 μm, respectively. SEM images of the NWs prepared at Ni^{2+} concentrations of 1.25, 5.00, and 10.00 mM are shown in Figure 2.

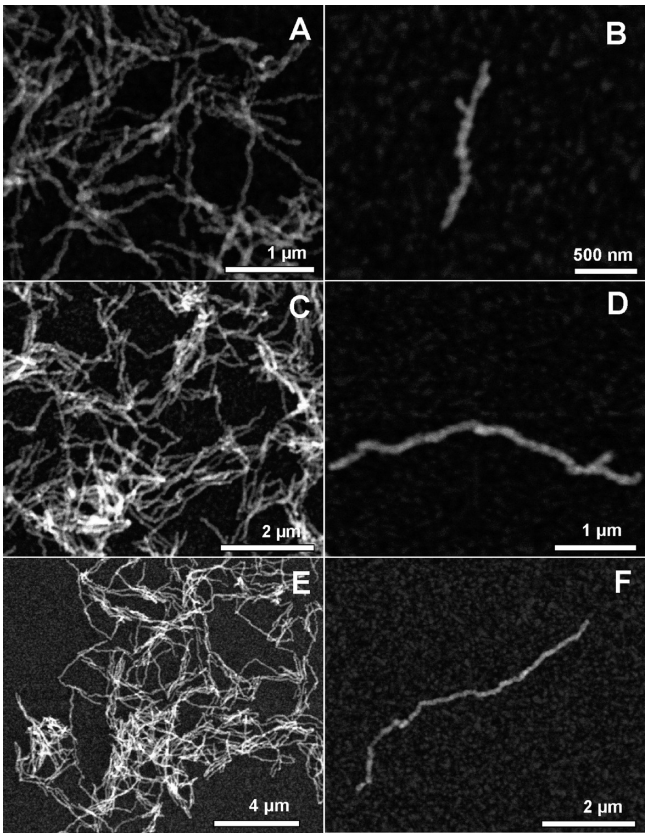

Figure 2. Large-area SEM images and corresponding images of single NWs synthesized at Ni^{2+} concentration of (A, B) 1.25 mM, (C, D) 5.00 mM, and (E, F) 10.00 mM.

We found that temperature plays an important role in determining the dimensions and morphology of the NWs. SEM images (Figure S2, Supporting Information) showed that higher the reduction temperature, the smaller the length and diameter of the NWs. Conditions and results of this set of experiments are summarized in Table 2 of the Supporting Information. Average diameters of the NWs synthesized at 90, 120, and 160 °C were 180 ± 7, 130 ± 5, and 100 ± 4 nm, respectively. Lengths of these samples were in the ranges of 20.00−25.00, 5.00−6.00, and 0.50−1.50 μm, respectively. These data correspond to average dimensions of 50 individual NWs. It is notable that temperature has a much greater influence on the nanowire dimensions than the concentration of Ni^{2+}. It is obvious from the SEM images that as the temperature increases, NWs appeared more like an assembly of nearly spherical particles than a continuous wire having a uniform surface. This kind of appearance was most prominent for the NWs prepared at 160 °C.

High-resolution (HR) TEM images of the NWs synthesized with 10 mM of Ni^{2+} at 160 °C clearly show (Figure 3A,B) the assembly of nearly spherical nickel nanoparticles. The observed *d*-spacing of 2.01 Å shown in Figure 3C corresponds to the (111)

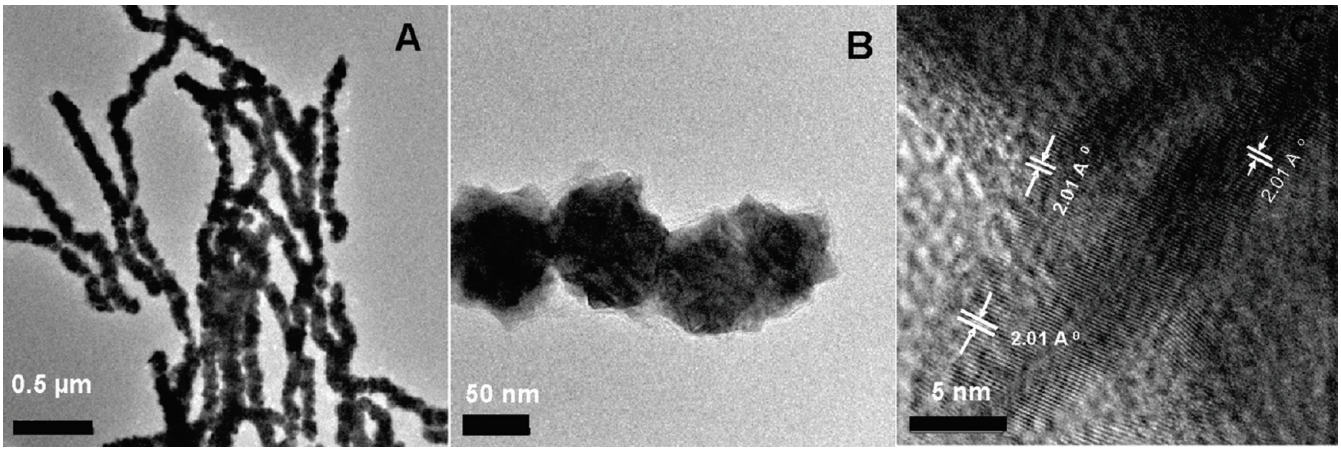

Figure 3. HRTEM images of (A) a collection of NWs and (B) magnified image of the tip of a single nanowire. (C) Lattice-resolved TEM image of a single nanowire.

lattice planes of face-centered cubic (fcc) nickel. We observed a significant change in the surface morphology of the Ni NWs prepared with varying amounts of hydrazine hydrate. We prepared NWs with 80, 200, and 500 μL of hydrazine hydrate solution at 10 mM concentration of Ni^{2+} at 90 °C. When the volume of hydrazine was 80 μL, the nanowire surface was smooth. As the amount of hydrazine increased, the surface becomes rough or nonuniform. This was obvious from the SEM images given in the Supporting Information (Figure S3).

Although the size and shape dependence of the optical properties of Au and Ag nanoparticles have been established theoretically[39a] and experimentally,[39b] reports on other transition metals are limited. Even though Ni nanoparticles of different morphologies were reported, very little is known about their optical properties.[40] NWs synthesized by this method exhibited unique features in their UV−vis spectra. Solid material appeared black, while a dilute dispersion in ethylene glycol, ethanol, or water had a faint blue color. Figure 4 shows the UV−vis spectra of Ni NWs prepared at various concentrations of Ni^{2+} (Figure 4A) and hydrazine (Figure 4B) as well as those at different temperatures (Figure 4C). Ni NWs synthesized at various Ni^{2+} concentrations showed a broad peak around 590−790 nm (Figure 4A). As the Ni^{2+} concentration is increased, the peak is significantly red-shifted. Lengths of the NWs prepared with Ni^{2+} concentrations of 1.25, 5.00, and 10.00 mM were 1.5−2.0, 3.0−3.5, and 5.0−6.0 μm, and diameters were 60 ± 4, 100 ± 5, and 130 ± 7 nm, respectively. Extinction peaks of these samples were found at around 592, 670, and 790 nm, respectively, which suggests a red shift in peak maximum with aspect ratio. Interestingly, when the nickel concentration was increased to 25 mM, the peak position was shifted beyond 1100 nm. NWs prepared with increasing amounts of hydrazine also showed systematic variations in the UV−vis spectrum as shown in Figure 4B. As the amount of hydrazine was increased, peak positions were shifted toward the lower-wavelength region.

NWs synthesized at 90, 120, and 160 °C, shown in Figure S2 in the Supporting Information, exhibited dramatic variation in the UV−vis features as shown in Figure 4C. Lengths of the NWs synthesized at 90, 120, and 160 °C were in the range of 20.0−25.0, 5.0−6.0, and 0.5−1.5 μm, and their diameters were 180 ± 7, 130 ± 5, and 100 ± 4 nm, respectively. NWs synthesized at 160 °C showed a broad and intense peak at around 625 nm. The extinction peak of NWs prepared at 120 °C was shifted to around 820 nm. NWs prepared at 90 °C had the largest average length and diameter, and the peak was shifted to the near-IR region.

The observed UV−vis features of Ni NWs can be due to both surface plasmon resonance (SPR) and scattering processes. Systematic changes observed in the UV−vis features of Ni NWs as a function of their dimensions may be an indication of the corresponding changes in their SPR. Theoretical calculations[41−43] show that spherical nickel nanoparticles exhibit one SPR feature in their UV−vis spectrum that can be distinguished from their interband transitions.[44] Size and shape dependence of SPR features of Ni nanopartcles are not studied in detail both theoretically and experimentally. Therefore, we do not assign the observed UV−vis feature to transverse and longitudinal plasmon modes. Calculations by Geddes and coworkers[45] showed that the extinction spectra of spherical Ni nanoparticles are dominated by the scattering component in the visible−near-IR region. Their calculation predicted a red shift in the extinction spectra of spherical Ni nanoparticles with increasing diameter. As explained earlier, a red shift was observed with increasing dimensions of Ni NWs synthesized by our method.

Nickel possesses an isotropic fcc crystal structure, and thus the formation of one-dimensional NWs is not expected without templates. As revealed by SEM and TEM, the surface of the NWs is not smooth and uniform and appeared as an assembly of nearly spherical particles. This prompted us to check whether the NWs are formed by assembly of smaller particles that might have formed during the early stages of growth. As mentioned in the Experimental Section, the reduction was completed and the NWs were found floating over the liquid surface within a few seconds after the addition of hydrazine. Moreover, during this period of time, the reaction mixture became highly nonuniform, resulting in a network-like appearance in the reaction mixture. This indicates that the nanowire formation is rapid. Due to this, we could not isolate any spherical nanoparticles as intermediates by a time-dependent extraction of the reaction mixture. Also, the supernatant of the reaction mixture was very clear and nanoparticles of any kind were not detected in it.

The roles of surfactant, templates, and magnetic field on Ni NW formation have been reported earlier.[28−36] Here, we found that the surfactant and magnetic field have negligible role in the formation of Ni NWs and they were formed even in the absence of surfactants

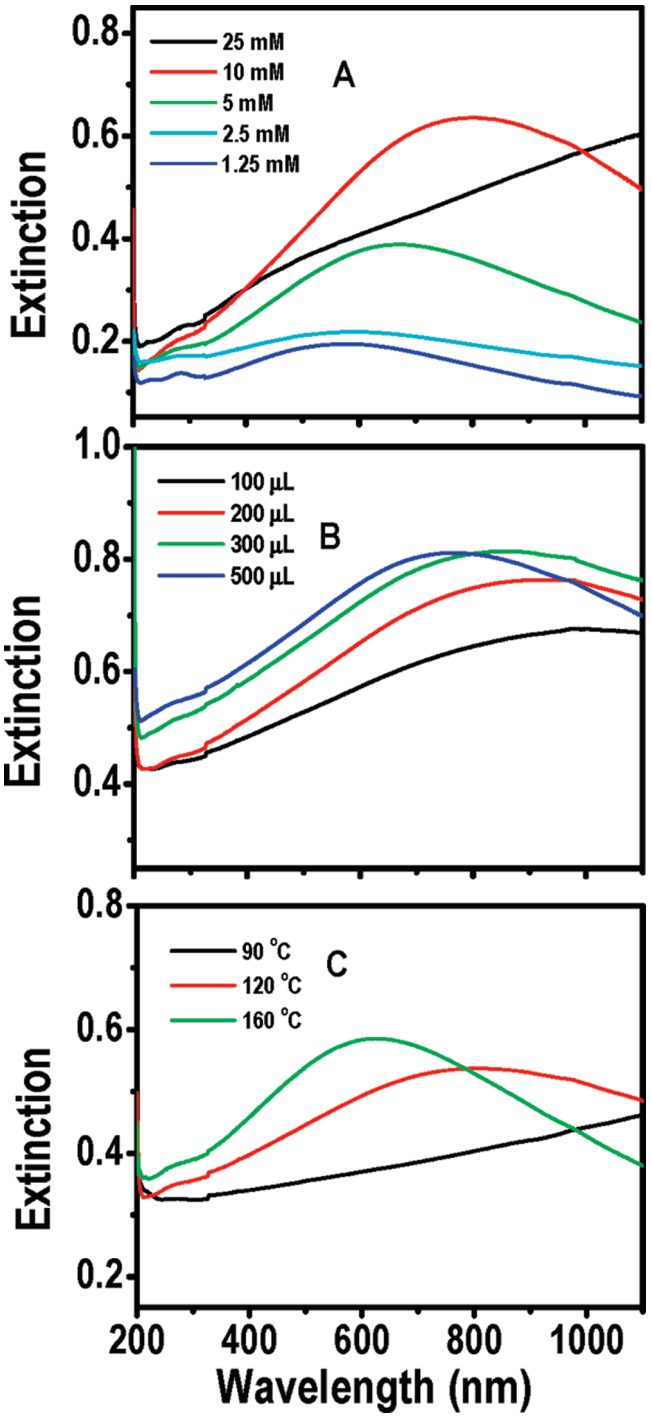

Figure 4. Extinction spectra of Ni NWs synthesized at different concentrations of (A) Ni^{2+} and (B) hydrazine and (C) at different temperatures.

and magnetic fields. We noted that the relative intensity, position, and width of the XRD peaks of the Ni NWs prepared with surfactants[28,33] were almost the same as those obtained in our case, that is, without any surfactants and magnetic fields. It should also be noted that the solvent and the reducing agent used in our experiments and some of the reports[31−35] are the same.

Even though we could not isolate any spherical nanoparticles as intermediates in our case, SEM and TEM data suggest that wires are formed by the assembly of nearly spherical nanoparticles. The particle assembly was visible in all our samples prepared at various Ni^{2+} concentrations and at different temperatures. TEM images (Figure 3A,B) of NWs prepared at 160 °C clearly show the assembly of nearly spherical particles. This kind of morphology becomes more clearly observable as the temperature of the reaction increases.

We suggest that the growth involves a two-step process: formation of the nearly spherical nanoparticles and their assembly to form wires. Oriented attachment (OA) can be a reason for the assembly of particles that might have formed initially. In the present case, small Ni nanocrystals might have been formed initially and they would have self-organized by sharing a common crystallographic orientation to reduce the surface energies of certain lattice planes, resulting in the formation of NWs.[46] Here, primary nanocrystals serve as the building blocks. Oriented attachment has been proven to generate irregularities in crystal structures as observed in our case.[47] Even though the OA mechanism was observed mostly in the presence of surfactants, studies on the hydrothermal synthesis of SnO_2 nanocrystals[48] and of CeO_2 nanorods[49] clearly show that this mechanism can occur in the absence of surfactants or capping agents. Further investigations are needed to understand the exact growth process, especially whether fresh nanoparticles are nucleated directly on a growing NW or grown particles assemble onto the growing NW.

Incorporation of multiple functionalities to the nanoparticles is one way to tailor their physical and chemical properties.[50] Here, we synthesized two types of functional NWs by incorporation of Te and ZnO on the nickel nanowire surfaces by a simple overgrowth reaction. Very rich growth of tellurium occurred on the nanowire surface. SEM images (Figure 5A,B) of the product clearly show the growth of thorn-like structures of tellurium on the nickel nanowire surface, which can be attributed to the inherently high tendency of tellurium for anisotropic crystal growth. Also, as can be seen from the SEM and TEM images, the nickel nanowire surface is nonuniform and contains several dips or troughs that can act as the nucleation sites for thorn-like overgrowth of tellurium. Ni K- and Te L-based EDAX images show distinct features (Figure 5C,D). The EDAX spectrum of Ni−Te NWs (Figure S4, Supporting Information) also confirms the presence of tellurium.

We used a solution-based method to make ZnO-coated Ni (Ni−ZnO) NWs using zinc acetate as the precursor. Figure 6 shows (A) the large-area image and (B) an image of a single Ni-ZnO nanowire. Figure 6 also depicts EDAX images of Ni−ZnO NWs, showing the intensities of (C) Ni L and (D) Zn L. The EDAX spectrum given in the Supporting Information (Figure S5) and X-ray diffraction analysis (Figure 7) also confirm the presence of zinc oxide on the NW surface. As in the case of Ni−Te NWs, surface roughness seems to be responsible for the nonuniform growth of ZnO particles on nanowire surface. We also tried ethylene glycol as the solvent since NWs can be dispersed for a longer time in ethylene glycol than in water and it will provide higher temperature, which favors the formation of ZnO coating. But we did not get ZnO coating with ethylene glycol, which may be due to the fact that ethylene glycol favors the nucleation and growth of small ZnO particles in the bulk liquid medium itself and not on the nanowire surfaces.

X-ray diffraction analysis of the pristine as well as the functional NWs has been done and the results are shown in Figure 7. The peaks at 2θ values of 44.12°, 51.45°, and 75.84° of pristine Ni NW may be assigned to (111), (200), and (220) planes, respectively, of face-centered cubic nickel (JCPDS card 04-

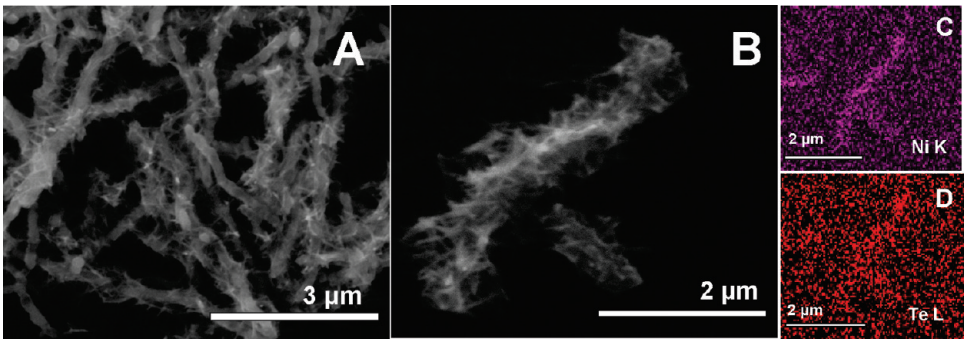

Figure 5. (A) Large-area SEM image of Ni−Te NWs and (B) corresponding image of a single nanowire. Also depicted are EDAX images of a single Ni−Te nanowire (shown in panel B), based on (C) Ni K and (D) Te L.

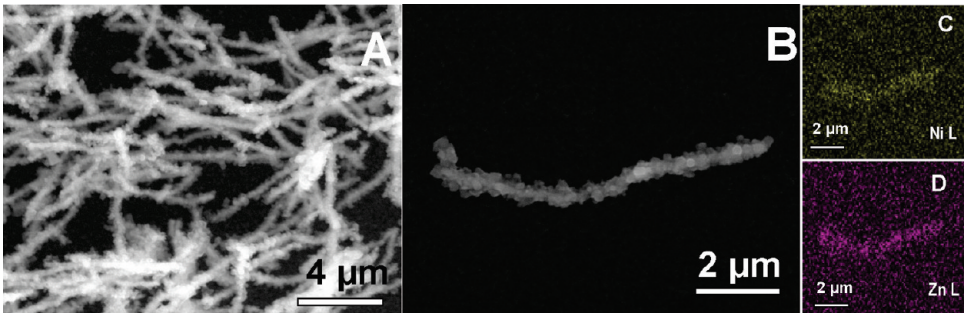

Figure 6. (A) Large-area SEM image of Ni−ZnO NWs and (B) corresponding image of a single nanowire. Also depicted are EDAX images of a single Ni−ZnO nanowire (shown in panel B), based on (C) Ni L and (D) Zn L.

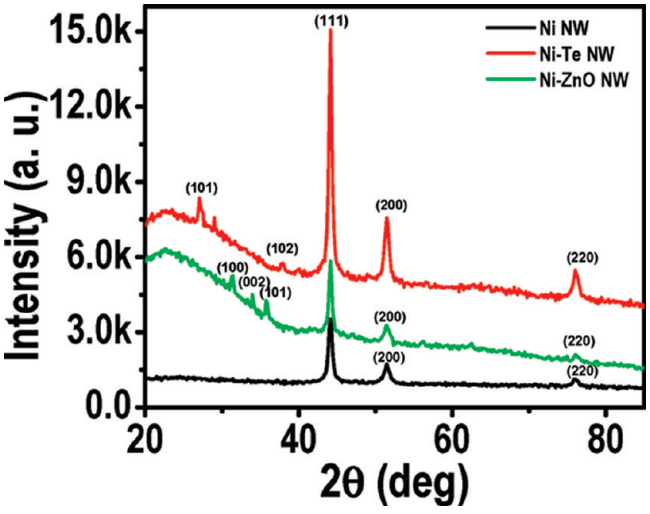

Figure 7. XRD patterns of pristine, tellurium-coated, and ZnO-coated Ni NWs.

0850). No other peaks were obtained, which proves that the product is pure and has no significant oxide. In the case of Ni−Te NWs, the peaks at 2θ values of 27.06°, 37.83°, and 40.08° were assigned to (101), (102), and (110) planes, respectively, of tellurium (JCPDS card 36-1452). The XRD pattern of Ni−ZnO NWs showed peaks at 31.40°, 33.94°, 35.74°, 56.24°, and 62.53°, corresponding to (100), (002), (101), (110), and (103) planes of ZnO (JCPDS card 79-0208).

Since ZnO has distinct Raman features, we could see the presence of ZnO coating by measuring the Raman spectra of the composite NWs. Also, we have created Raman images by collecting the spectral intensities in the ranges of 200−2500 (Figure 8A), 400−500 (Figure 8B), and 1000−1200 cm^{-1} (Figure 8C). During the synthesis of Ni−ZnO nanowire, it is expected to form a thin layer of NiO on the nickel nanowire surface. Even though the NiO layer was not characterized in the XRD analysis, Raman spectra (Figure 8D) showed the features of NiO. The observed intensity in Figure 8A corresponds to the combined intensity of different phonon modes of both ZnO and NiO. Figure 8A (inset) is the optical image of the tellurium NWs used for Raman imaging. Figure 8B shows the intensity of E_2 (high) mode of the ZnO occurring at 428 cm^{-1} (marked as 1 in Figure 8D).[51] The peak at around 550 cm^{-1} in the Raman spectrum is due to the longitudinal optical (LO) phonon mode of NiO. The observed intensity in Figure 8C is due to the combination phonon mode (2LO) of NiO occurring at 1102 cm^{-1} (marked as 2 in Figure 8D).[52]

It has been shown that highly anisotropic nanostructures are suitable candidates for SERS applications.[53] The enormous enhancements in the Raman signals of molecules in SERS has practical utility only in metals like Ag, Au, and Cu because their surface plasmons can be easily excited by visible or near-infrared (NIR) radiation.[54]Au and Ag nanoparticles have been extensively used for SERS-based sensing of biomolecules.[55a] Since the Ni NWs are highly anisotropic in nature and have rough surfaces, we studied the SERS activity of these NWs using crystal violet (CV) as an analyte. For that, we collected the Raman spectra of adsorbed CV molecules at different concentrations (Figure 9).

We could get Raman features of CV adsorbed on Ni NWs even at a concentration of 10^{-5} M, which was not observed in the

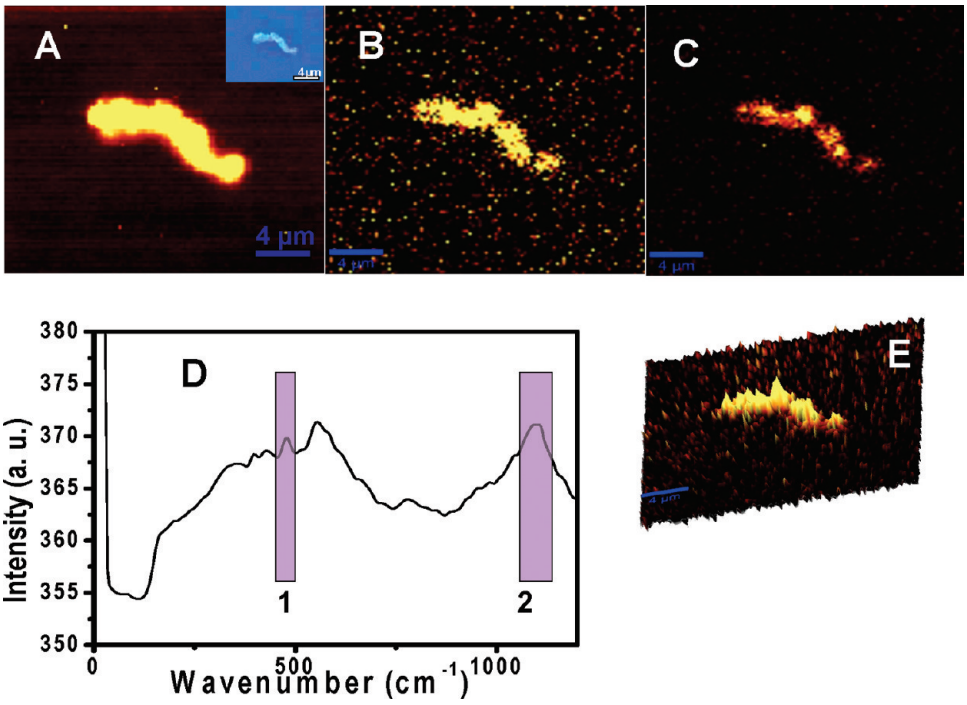

Figure 8. Raman images of the Ni−ZnO nanowire created by collecting the spectral intensities between (A) 200 and 2500 cm^{-1}, (B) 400 and 500 cm^{-1}, and (C) 1000 and 1200 cm^{-1}. (D) Raman spectrum of the Ni−ZnO NWs. (E) Three-dimensional view of the Raman image shown in panel A.

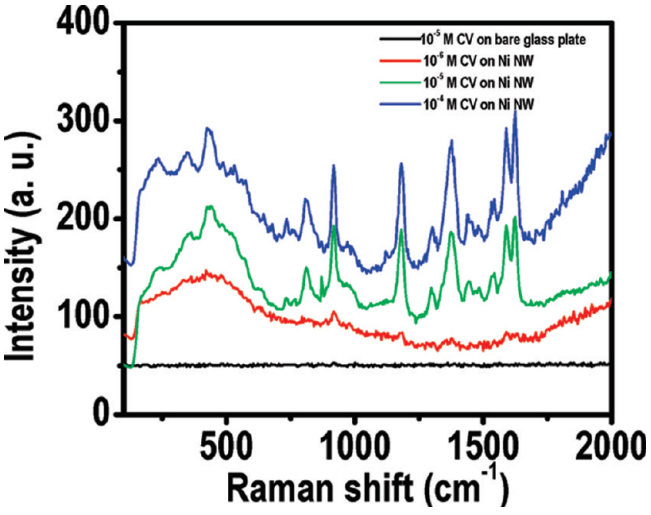

Figure 9. Raman spectra of CV of various concentrations adsorbed on Ni NWs.

case of a bare glass plate. Even though the signal intensity was poor, we observed the Raman features of adsorbed CV on Ni nanowire at a concentration of 10^{-6} M (Figure 9). From this it is clear that Ni NWs gives significant signal intensity up to a concentration of 10^{-6} M in the case of CV. The enhancement factor has been estimated by the method given in ref 55b, and the value was about 1.7×10^4 for the 1593 cm^{-1} feature. Experimental[56] as well as theoretical[57] studies show that nickel nanowire arrays exhibit SERS activity and an enhancement factor of 10^4-10^5 can be obtained. Theoretical calculations show that a lightning-rod effect in the electromagnetic mechanism can enhance the SERS activity of Ni NWs.[57]

5. CONCLUSIONS

In conclusion, we synthesized Ni NWs of high purity in good yield using a simple wet-chemical reduction route without the assistance of any surfactants, template, or external magnetic field. We think that oriented attachment of nanoparticles is responsible for the nanowire formation, but the exact growth mechanism could not be observed by time-dependent sampling of the nanostructures. Optical absorption features of Ni NWs have been studied as a function of nanowire dimensions. By use of Ni NWs as template, tellurium- and zinc oxide-coated Ni NWs have been prepared by simple wet-chemical overgrowth processes. The pristine as well as functional NWs are expected to be useful candidates for practical applications. We demonstrated the SERS activity of pristine Ni NWs using crystal violet as the probe molecule.

■ ASSOCIATED CONTENT

Supporting Information. Five figures, showing EDAX spectra of pristine, Ni−Te, and Ni−ZnO NWs and SEM images of Ni NWs synthesized at different temperatures and with different amounts of hydrazine hydrate, and two tables, summarizing the experimental conditions and results. This material is available free of charge via the Internet at http://pubs.acs.org.

■ AUTHOR INFORMATION

Corresponding Author
*E-mail pradeep@iitm.ac.in; fax + 91-44 2257-0545.

■ ACKNOWLEDGMENT

We thank the Department of Science and Technology, Government of India, for constantly supporting our research program on nanomaterials.

REFERENCES

(1) (a) Murray, C. B.; Kagan, C. R.; Bawendi, M. G. *Science* **1995**, *270*, 1335–1338. (b) Zeng, H.; Li, J.; Wang, Z. L.; Liu, J. P.; Sun, S. *Nature* **2002**, *420*, 395. (c) Shevchenko, E. V.; Talapin, D. V.; Rogach, A. L.; Kornowski, A.; Haase, M.; Weller, H. *J. Am. Chem. Soc.* **2002**, *124*, 12480.

(2) Raj, K.; Moskowitz, R.; Casciari, R. *J. Magn. Magn. Mater.* **1995**, *149*, 74.

(3) (a) Gupta, P. K.; Hung, C. T. *Life Sci.* **1989**, *44*, 175–186. (b) Giri, J.; Ray, A.; Dasgupta, S.; Datta, D.; Bahadur, D. *Biomed. Mater. Eng.* **2003**, *13*, 387.

(4) Huajun, Z.; Jinhuan, Z.; Zhenghai, G.; Wei, W. *J. Magn. Magn. Mater.* **2008**, *320*, 565–570.

(5) Cordente, N.; Respaud, M.; Senocq, F.; Casanove, M. J.; Amiens, C.; Chaudret, B. *Nano Lett.* **2001**, *1*, 565–568.

(6) Tao, F.; Guan, M.; Jiang, Y.; Zhu, J.; Xu, Z.; Xue, Z. *Adv. Mater.* **2006**, *18*, 2161–2164.

(7) Ma, S.; Srikanth, V. V. S. S.; Maik, D.; Zhang, G. Y.; Staedlar, T.; Jiang, X. *Appl. Phys. Lett.* **2009**, *94*, No. 013109.

(8) Libor, Z.; Zhang, Q. *Mater. Chem. Phys.* **2009**, *114*, 902–907.

(9) Bradley, J. S.; Tesche, B.; Busser, W.; Maase, M.; Reetz, M. T. *J. Am. Chem. Soc.* **2000**, *122*, 4631–4636.

(10) Hong, X.; Wang, Y. *J. Nat. Gas Chem.* **2009**, *18*, 98–103.

(11) (a) Byrne, F.; Mello, A. P.; Whelan, A.; Mohamed, B. M.; Davies, A.; Gun'ko, Y. K.; Coey, J. M. D.; Volkov, Y. *J. Magn. Magn. Mater.* **2009**, *321*, 1341–1345. (b) Hultgren, A; Tanase, M; Chen, C. S.; Meyer, G. J.; Reich, D. H. *J. Appl. Phys.* **2003**, *93*, 7554–7556.

(12) Hultgren, A.; Tanase, M.; Felton., E. J.; Bhadriraju, K.; Salem, A. K.; Chen, C. S.; Reich, D. H. *Biotechnol. Prog.* **2005**, *21*, 509–515.

(13) Choi, D.; Fung, A.; Moon, H.; Ho, A.; Chen, Y.; Kan, E.; Rheem, Y.; Yoo, B.; Myung, M. *Biomed. Microdevices* **2007**, *9*, 143–148.

(14) Jorritsma, J.; Mydosh, J. A. *J. Appl. Phys.* **1998**, *84*, 901–906.

(15) Grigoriev, S. V.; Chumakov, A. P.; Syromyatnikov, A. V.; Grigorieva, N. A.; Okorokov, A. I.; Napol'skii, K. S.; Roslyakov, I. V.; Eliseev, A. A.; Lukashin, A. V.; Eckerlebe, H. *Phys. Solid State* **2010**, *52*, 1080–1086.

(16) Nielsch, K.; Wehrspohn, R. B.; Barthel, J.; Kirschner, J.; Fischer, S. F.; Kronmuller, H.; Schweinbock, T.; Weiss, D.; Gosele, U. *J. Magn. Magn. Mater.* **2002**, *249*, 234–240.

(17) Rahman, I. Z.; Razeeb, K. M.; Rahnan, M. A.; Kamruzzaman, Md. *J. Magn. Magn. Mater.* **2003**, *262*, 166–169.

(18) Oh, B. K.; Park, S.; Millstone, J. E.; Lee, S. W.; Lee, K. B.; Mirkin, C. A. *J. Am. Chem. Soc.* **2006**, *128*, 11825–11829.

(19) Lee, K. B.; Park, S.; Mirkin, C. A. *Angew. Chem., Int. Ed.* **2004**, *43*, 3048–3050.

(20) Wu, C. G.; Lin, H. L.; Shau, N. L. *J. Solid State Electron.* **2006**, *10*, 198–202.

(21) Talapatra, S.; Tang, X.; Padi, M.; Kim, T.; Vajtai, R.; Sastry, G. V. S.; Shima, M.; Deevi, S. C.; Ajayan, P. M. *J. Mater. Sci.* **2009**, *44*, 2271–2275.

(22) (a) Thongmee, S.; Pang, H. L.; Yi, J. B.; Ding, J.; Lin, J. Y.; Van, L. H. *Acta Mater.* **2009**, *57*, 2482–2487. (b) Ahmed, J.; Sharma, S.; Ramanujachary, K. V.; Lofland, S. E.; Ganguly, A. K. *J. Colloid Interface Sci.* **2009**, *336*, 814–819.

(23) Chen, Y.; Yan, H.; Li, X. H.; Li, W.; Zhang, J. W.; Zhang, X. Y. *Mater. Lett.* **2006**, *60*, 245–247.

(24) Narayanan, T. N.; Shaijumon, M. M.; Ajayan, P. M.; Anantharaman, M. R. *Nanoscale Res. Lett.* **2010**, *5*, 164–168.

(25) Zhang, S.; Zeng, H. C. *Chem. Mater.* **2010**, *22*, 1282–1284.

(26) (a) Kudryavstev, A. A. *The Chemistry and Technology of Selenium and Tellurium*; Collet's Ltd: London, 1974. (b) Klingshirn, C. *Phys. Status Solidi B* **2007**, *244*, 3027–3073.

(27) (a) Wen, S.; Szpunar, J. A. *Micro Nano Lett.* **2006**, *1*, 89–93. (b) Bently, A. K.; Farhoud, M.; Ellis, A. B.; Licensky, G. C.; Nickel, A. L.; Crone, W. C. *J. Chem. Educ.* **2005**, *82*, 765–768.

(28) Niu, H.; Chen, Q.; Ning, M.; Jia, Y.; Wang, X. *J. Phys. Chem. B* **2004**, *108*, 3996–3999.

(29) Liu, P.; Li, Z.; Zhao, B.; Yadian, B.; Zhang, Y. *Mater. Lett.* **2009**, *63*, 1650–1652.

(30) Zhang, L. Y.; Wang, J.; Wei, L. M.; Liu, P.; Wei, H.; Zhang, Y. F. *Nano Micro Lett.* **2009**, *1*, 49–52.

(31) Much, R. A.; Gedanken, A. *Chem.—Eur. J.* **2008**, *14*, 10115–10122.

(32) Hu, X.; Yu, J. C. *Chem. Mater.* **2008**, *20*, 6743–6749.

(33) Wang, D. P.; Sun, D. B.; Yu, H. Y.; Qiu, Z. G.; Ming, H. M. *Mater. Chem. Phys.* **2009**, *113*, 227–232.

(34) Hu, H.; Sugawara, K. *Chem. Phys. Lett.* **2009**, *477*, 184–188.

(35) Zhang, G.; Zhang, T.; Lu, X.; Wang, W.; Qu, J.; Li, X. *J. Phys. Chem. C* **2007**, *111*, 12663–12668.

(36) Jia, F.; Zhang, L.; Shang, X.; Yang, Y. *Adv. Mater.* **2008**, *20*, 1050–1054.

(37) Lin, Z. H.; Yang, Z.; Chang, H. T. *Cryst. Growth Des.* **2008**, *8*, 351–357.

(38) Xi, G.; Liu, Y.; Wang, X.; Liu, X.; Peng, Y.; Qian, Y. *Cryst. Growth Des.* **2006**, *6*, 2567–2570.

(39) (a) Link, S.; Mohamed, M. B.; El-Sayed, M. A. *J. Phys. Chem. B* **1999**, *103*, 3073–3077. (b) Jana, N. R.; Gearheart, L.; Murphy, C. J. *J. Phys. Chem. B* **2001**, *105*, 4065–4067.

(40) Shi, J. B.; Chen, Y. C.; Lee, C. W.; Lin, Y. T.; Wu, C.; Chen, C. J. *Mater. Lett.* **2008**, *62*, 15–18.

(41) Creighton, J. A.; Eadon, D. G. *J. Chem. Soc., Faraday Trans.* **1991**, *87*, 3881.

(42) Yeshchenko, O. A.; Dmitruk, I. M.; Alexeenko, A. A.; Dmytruk, A. M. *J. Phys. Chem. Solids* **2008**, *69*, 1615–1622.

(43) Amekura, H.; Takeda, Y.; Kishimoto, N. *Nucl. Instrum. Methods Phys. Res., Sect. B* **2004**, *222*, 96–104.

(44) Amekura, H.; Takeda, Y.; Kitazawa, H.; Kishimoto, N. *Proc. SPIE* **2003**, *4977*, 639.

(45) Zhang, Y.; Dragan, A.; Geddes, C. D. *J. Phys. Chem. C* **2009**, *113*, 15811–15816.

(46) Zhang, J.; Huang, F.; Lin, Z. *Nanoscale* **2010**, *2*, 18–34.

(47) Huang, F.; Zhang, H.; Banfield, J. F. *Nano Lett.* **2003**, *3*, 373–378.

(48) Lee, E. J. H.; Ribeiro, C.; Longo, E.; Leite, E. R. *J. Phys. Chem. B* **2005**, *109*, 20842–20846.

(49) Du, N.; Zhang, H.; Chen, B.; Ma, X.; Yang, D. *J. Phys. Chem. C* **2007**, *111*, 12677–12680.

(50) (a) Cao, Y. W.; Jin, R.; Mirkin, C. A. *J. Am. Chem. Soc.* **2001**, *123*, 7961–7962. (b) Mullin, M. P.; Murphy, C. J. *Nano Lett.* **2002**, *2*, 1235. (c) Yang, J.; Lee, J. Y.; Chen, L. X.; Too, H. P. *J. Phys. Chem. B* **2005**, *109*, 5468. (d) Sajanlal, P. R.; Pradeep, T. *Langmuir* **2010**, *26*, 8901–8907.

(51) Ozgur, U.; Alivov, Y. I.; Liu, C.; Teke, A.; Reshchikov, M. A.; Dogan, S.; Avrutin, V.; Cho, S.-J.; Morkoc, H. *J. Appl. Phys.* **2005**, *98*, 041301.

(52) Varghese, B.; Reddy, M. V.; Yanwu, Z.; Lit, C. S.; Hoong, T. C.; Rao, G. V. S.; Chowdari, B. V. R.; Wee, A. T. S.; Lim, C. T.; Sow, C. H. *Chem. Mater.* **2008**, *20*, 3360–3367.

(53) (a) Imura, K.; Okamoto, H.; Hossain, M. K.; Kitajima, M. *Nano Lett.* **2006**, *6*, 2173–2176. (b) Qin, L.; Zou, S.; Xue, C.; Atkinson, A.; Schatz, G. C.; Mirkin, C. A. *Proc. Natl. Acad. Sci. U.S.A.* **2006**, *103*, 13300–13303.

(54) Ren, B.; Liu, G. K.; Lian, X. B.; Yang, Z. L.; Tian, Z. Q. *Anal. Bioanal. Chem.* **2007**, *388*, 29–45.

(55) (a) Kim, K; Lee, H. S.; Kim, N. H. *Anal. Bioanal. Chem.* **2007**, *388*, 81–88. (b) Kumar, G. V. P.; Shruthi, S.; Vibha, B.; Reddy, B. A. A.; Kundu, T. K.; Narayana, C. *J. Phys. Chem. C* **2007**, *111*, 4388–4392.

(56) Saur, G.; Brehm, G.; Schneider, S.; Graener, H.; Seifert, G.; Nielsch, K.; Goring, J. C. P.; Gosele, U.; Miclea, P.; Wehrspohn, R. B. *Appl. Phys. Lett.* **2006**, *88*, No. 023106.

(57) Zhilin, Y.; Deyin, W.; Jianlin, Y.; Jianqiang, H.; Bin, R.; Haiguang, Z.; Zhongqun, T. *Chin. Sci. Bull.* **2002**, *47*, 1983–1986.